Inverted light sheet microscope for imaging mouse pre-implantation development

Petr Strnad, Stefan Gunther, Judith Reichmann, Uros Krzic, Balint Balazs, Gustavo de Medeiros, Nils Norlin, Takashi Hiiragi[2], Lars Hufnagel, Jan Ellenberg

European Molecular Biology Laboratory
Cell Biology and Biophysics Unit
69117 Heidelberg
Germany

[2]European Molecular Biology Laboratory
Developmental Biology Unit
69117 Heidelberg
Germany

Correspondence should be addressed to J.E. (jan.ellenberg@embl.de).

Despite its importance for understanding human infertility and congenital diseases, early mammalian development has remained inaccessible to *in toto* imaging. We developed an inverted light sheet microscope which enabled us to image mouse embryos from zygote to blastocyst, computationally track all cells and reconstruct a complete lineage tree of mouse pre-implantation development. We used this unique dataset to show that the first cell fate specification occurs at 16-cell stage.

In toto imaging of biological model organisms such as worm[1], fly[2] and fish[3] has revolutionized our understanding of cell division and cell fate specification in their early development. However, due to high light sensitivity and demanding *in vitro* culture requirements *in toto* imaging of mammalian pre-implantation embryos has not been possible and a number of important questions, including the time of cell fate specification, remain controversial[4–12]. In addition, the high degree of variability in early mammalian development[13] requires statistical analysis of accurately reconstructed cell lineages of several embryos to draw solid conclusions. Light sheet microscopy[14] is the tool of choice to image large and light-sensitive specimens. Because the excitation light is restricted to the focal plane, light exposure and phototoxicity are minimized. For a typical mammalian pre-implantation embryo of 80-100 µm in diameter this allows the light dose to be reduced by about two orders of magnitude compared to standard confocal or two-photon microscopy without compromising resolution[15]. The need to place the specimen in the narrow space between illumination and detection objectives, however, has led to light sheet microscope designs where the specimen is held vertically by embedding into agarose cylinders[14] or small capillaries[16], which is incompatible with mammalian embryo development. Alternative light-sheet microscope configurations which eliminate the requirement of sample embedding have been developed[1,17–20], but none of them is well-suited for high-resolution imaging of many pre-implantation embryos in parallel (Supplementary Discussion). Although live imaging of mouse pre-implantation development was conducted before by confocal microscopy[21–24] none of these studies successfully imaged complete development from zygote to blastocyst. Furthermore, light sheet microscopy has so far only been used to image post-implantation mouse embryos[19,20].

To overcome this limitation we developed an inverted light sheet microscope where both the illumination and the detection objective face upwards in an immersion water reservoir (Fig. 1a and Supplementary Fig. 1). The specimen is held by gravity in a long narrow channel of a microscope slide sized holder (Fig. 1b) and can therefore be lowered between the two objectives (Fig. 1c), similar to a standard glass-bottom dish on an inverted microscope. Since the transparent plastic of the sample channel has the refractive index of water, the specimen is optically fully accessible for high resolution immersion objectives, yet physically isolated from the immersion medium and can be maintained in standard microdrop *in vitro* embryo culture (Fig. 1c). Full environmental incubation of the imaging system (Supplementary Fig. 2) allows maintaining stable temperature and atmosphere composition. Furthermore, free movement along the long axis of the specimen channel allows placing many embryos in a row for high-throughput imaging (Fig. 1b). For maximum multicolor imaging speed we implemented simultaneous imaging of separated EGFP and mCherry fluorescence signals on a single camera chip (Supplementary Fig. 3). Our asymmetric optical design with a lower numerical aperture light sheet generating objective and a high collection efficiency detection objective provides resolution comparable to confocal microscopy (Supplementary Fig. 4) at highly reduced light dose.

Mammalian development from the fertilized zygote to the fully grown blastocyst with 64 cells requires approximately three days. At this time, the first cell fate decisions have been taken and the first two early

embryonic lineages are segregated: the trophectoderm (TE), which forms extraembryonic tissue, and the inner cell mass (ICM), which gives rise to the embryo proper and is the source of embryonic stem cells[25]. The two lineages can be clearly distinguished in the blastocyst as only TE cells are in direct contact to the outside environment. For *in toto* reconstruction of pre-implantation development, it is necessary to track all cells through the first six divisions, for which we chose the chromosomal protein histone 2B (H2B) tagged with a red fluorescent protein (mCherry) as a marker[26]. To assign cell fates at the blastocyst stage, we crossed mice with the chromosomal marker (H2B-mCherry) to mice expressing with a cell surface marker (green fluorescent protein with a myristylation sequence[27]; mG). After optimizing the spatial and temporal sampling to reach sufficient resolution to track every blastomere division reliably (Fig. 2a, b and Supplementary Videos 1 and 2), we verified that three days of time-lapse imaging did not affect normal embryonic development. The high throughput of our system allowed us to image a total of 139 embryos in seven three-day microscope runs (20 embryos/run) with unprecedented spatiotemporal resolution. Out of the 129 embryos with two pronuclei at the start of time-lapse, 20% (26) expressed both fluorescent markers, 98% (126) cavitated and 93% (120) formed expanded blastocysts with a well-defined inner cavity. In addition, the tracked embryos had a division timing[28] and number of ICM cells[12] comparable to *in vitro* cultured embryos (Online Methods) and healthy pups were born after transfer of imaged embryos into pseudopregnant females (Supplementary Fig. 5). This indicates that the illumination dose of our light sheet system did not delay or noticeably affect *in vitro* pre-implantation development. By contrast, embryos imaged at comparable spatiotemporal resolution using a confocal microscope were arrested already before the eight cell stage and did not develop further (Supplementary Fig. 6).

To automatically derive cell trajectories from the microscopy data we developed a two-step segmentation and tracking pipeline (Online Methods) of the chromosomal H2B fluorescence signal. In the first step, chromosomes were segmented using machine learning in Ilastik[29] to derive nuclear regions and calculate the chromosome mass centroids. In the second step, these centroids were automatically aligned[30] and tracked to reconstruct a complete embryonic cell lineage (Fig. 2c). We verified all final tracks manually and corrected in rare cases (Online Methods). The resulting cell trajectories (Fig. 2d and Supplementary Video 3) were then used to computationally reconstruct the complete lineage tree for each embryo. Cell fate, i.e. belonging to the TE or ICM, was assigned at ~64-cell stage based on cell contact to the outside environment using the cell surface signal which was imaged in addition to chromosomes for this purpose at the end of the time-lapse (Fig. 3a-c and Supplementary Fig. 7).

After removing data sets where embryos had moved out of focus or rotated too rapidly for automatic alignment, we obtained fully analyzable 4D *in toto* imaging data sets for 12 double heterozygote embryos and performed complete lineage tracking and TE and ICM fate assignments (Supplementary Data). This unique data set put us in a position to address the long standing question[5,7,10,31,32] of when the contribution of blastomeres to different cell fates first becomes non-random in mouse embryos. To this end, we backtracked cell lineages and calculated the percentage of TE or ICM cells derived from each branch of the tree (Fig. 3c and Supplementary Video 4). This analysis revealed that until the 8-cell stage over 90% of blastomeres still gave rise to both TE and ICM cells (87 out of 96 8-cell stage blastomeres), while at the 16-cell stage already over half of the blastomeres exclusively gave rise to one or the other lineage (102 out of 192 16-cell stage blastomeres; Fig. 3c and Supplementary Fig. 7). To test if such behavior could occur randomly, we compared our experimental data with 100,000 lineage trees with randomized cell fates (Fig. 3d,e) and calculated the probability that the experimentally observed lineage segregation had occurred by chance (Online Methods and Supplementary Note). Plotting this probability for each level of the tree allowed assessing the time of non-random cell fate distribution in every embryo (Fig. 3f). The contribution of blastomeres to different progeny fates did not significantly deviate from random at the 2-, 4- and 8-cell stage for all embryos (p-value > 0.01; Fig. 3g and Supplementary Fig. 8). At the 16-cell stage however contributions became significantly non-random for 7 out of 12 (p-value < 0.01) and for all embryos by the 32-cell stage (Fig. 3g and Supplementary Fig. 8). The variability at the 16-cell stage is consistent with the variable number of inside cells reported at this stage[12,21]. By integrating data from all 12 embryos and calculating global probabilities for each level of the lineage tree (Fig. 3g) our statistical test could detect even a slight bias in the contribution of individual blastomeres to TE or ICM fate that would not be detected at the single embryo level. Up to the 8-cell stage the probabilities obtained for each embryo are distributed evenly between zero and one (Fig. 3g), strongly arguing against any bias in contributing to a specific lineage. This distribution as well as the combined probability for all embryos then showed a sharp transition from the 8- to 16-cell stage (Fig. 3g), allowing us to conclude that the 16-cell embryo is the earliest stage where blastomeres are significantly biased in their contributions to TE or ICM cell fates. We further mined our dataset and, consistent with earlier observations[21,33], found that the spindle axes in the embryos became significantly non-random (p-value < 0.01) with a bias towards perpendicular orientation from the embryo surface for the critical 8- to 16-cell division and that such division orientation correlated with cell fate (Supplementary Fig. 9-12 and Supplementary Results).

Our newly developed inverted light sheet microscope and computational data analysis pipeline provide the tools to routinely generate complete lineage trees of tens of mouse embryos in parallel per experiment. Using this technology we succeeded to conduct the first *in toto* imaging of mammalian development from zygote to blastocyst. Our inverted light sheet microscope can be applied to a broad range of biological samples, such as single mammalian cells, embryos of other species and recently developed organoid models (Supplementary Discussion). This opens exciting new perspectives to map the key regulatory molecules of cell division and cell fate specification onto digital 4D atlases of pre-implantation embryos and come to an integrated spatio-temporal understanding of early mammalian development at the molecular level. Future improvements in light sheet

microscopy[34] that do not increase light dose, such as image aberration correction using adaptive optics[35], should allow us to drive our level of understanding from the cellular to the organellar, and ultimately to the single molecule level in living mammalian embryos.

Methods

Methods are available in the online version of the paper.

Acknowledgments

We thank the mechanical and electronics workshop of the European Molecular Biology Laboratory (EMBL) for customized hardware, B. Klaus and S. Anders for help with statistical analysis, M. Eguren for cell fate assignment, E. Korotkevich for help with confocal imaging, B. Nijmeijer for mouse genotyping and EMBL's laboratory of animal resources for excellent support with mouse strains. The EMBL Advanced Light Microscopy Facility is acknowledged for support in image acquisition and analysis. This work was supported by funds from the German Research Foundation within in the priority program SPP 1384 "Mechanisms of genome haploidization" (DFG EL 246/4-2) to J.E., by the European Union EU-FP7-MitoSys (Grant Agreement 241548) to J.E, and by the European Molecular Biology Laboratory (P.S., S.G., J.R., U.K., B.B., G.M., N.N. T.H., L.H., J.E.). P.S. was further supported by the EMBL Interdisciplinary Postdoc Programme (EIPOD) under Marie Curie Actions COFUND.

Author contributions

J.E. supervised the work and originally conceived the project.
L.H. and P.S. contributed to conception and design of the work.
P.S. performed the experiments, designed and constructed the microscope and carried out the statistical analysis of the data as well as computer simulations.
S.G. developed the software for cell tracking and applied it to the data.
J.R. contributed to data acquisition and optimization of the microscope.
T.H. supervised the embryological aspects of the work and carried out cell fate assignments.
B.B., G.d.M., N.N. developed and wrote the microscope software under the supervision of L.H.
U.K. helped in the initial design of the microscope.
J.E. and P.S. wrote the manuscript.
All authors contributed to the design of the microscope or the experiments and interpretation of the data and read and approved the final manuscript.

Competing financial interests

The authors declare no competing financial interests.

Editor's Summary

An inverted light sheet microscope enables pre-implantation mouse embryos to be imaged from zygote to blastocyst with minimal photodamage and high resolution for automatic lineage tree reconstruction allowing new insight into mammalian development and cell fate specification.

References

1. Wu, Y. *et al. Proc. Natl. Acad. Sci. U. S. A.* **108,** 17708–17713 (2011).
2. Krzic, U., Gunther, S., Saunders, T. E., Streichan, S. J. & Hufnagel, L. *Nat. Methods* **9,** 730–733 (2012).
3. Keller, P. J., Schmidt, A. D., Wittbrodt, J. & Stelzer, E. H. K. *Science* **322,** 1065–1069 (2008).
4. Piotrowska, K., Wianny, F., Pedersen, R. A. & Zernicka-Goetz, M. *Development* **128,** 3739–3748 (2001).
5. Tabansky, I. *et al. Curr. Biol.* **23,** 21–31 (2013).
6. Zernicka-Goetz, M. *Nat. Rev. Mol. Cell Biol.* **6,** 919–928 (2005).
7. Plachta, N., Bollenbach, T., Pease, S., Fraser, S. E. & Pantazis, P. *Nat. Cell Biol.* **13,** 117–123 (2011).
8. Motosugi, N., Bauer, T., Polanski, Z., Solter, D. & Hiiragi, T. *Genes Dev.* **19,** 1081–1092 (2005).
9. Gardner, R. L. *Development* **128,** 839–847 (2001).
10. Hiiragi, T. *et al. Int. J. Dev. Biol.* **50,** 581–586; discussion 586–587 (2006).
11. Piotrowska-Nitsche, K., Perea-Gomez, A., Haraguchi, S. & Zernicka-Goetz, M. *Development* **132,** 479–490 (2005).
12. Dietrich, J.-E. & Hiiragi, T. *Development* **134,** 4219–4231 (2007).
13. Dietrich, J. E. & Hiiragi, T. *Cells Tissues Organs* **188,** 46–51 (2008).
14. Huisken, J., Swoger, J., Del Bene, F., Wittbrodt, J. & Stelzer, E. H. K. *Science* **305,** 1007–1009 (2004).
15. Weber, M. & Huisken, J. *Curr. Opin. Genet. Dev.* **21,** 566–572 (2011).
16. Kaufmann, A., Mickoleit, M., Weber, M. & Huisken, J. *Development* **139,** 3242–3247 (2012).
17. McGorty, R. *et al. Opt. Express* **23,** 16142–16153 (2015).
18. Capoulade, J., Wachsmuth, M., Hufnagel, L. & Knop, M. *Nat. Biotechnol.* **29,** 835–839 (2011).
19. Ichikawa, T. *et al. PloS One* **8,** e64506 (2013).
20. Udan, R. S., Piazza, V. G., Hsu, C.-W., Hadjantonakis, A.-K. & Dickinson, M. E. *Development* **141,** 4406–4414 (2014).
21. Watanabe, T., Biggins, J. S., Tannan, N. B. & Srinivas, S. *Development* **141,** 2279–2288 (2014).
22. Morris, S. A. *et al. Proc. Natl. Acad. Sci. U. S. A.* **107,** 6364–6369 (2010).
23. Xenopoulos, P., Kang, M., Puliafito, A., Di Talia, S. & Hadjantonakis, A.-K. *Cell Rep.* **10,** 1508–1520 (2015).
24. Dietrich, J.-E. *et al. EMBO Rep.* **16,** 1005–1021 (2015).
25. Posfai, E., Tam, O. H. & Rossant, J. *Curr. Top. Dev. Biol.* **107,** 1–37 (2014).
26. Abe, T. *et al. Genesis* **49,** 579–590 (2011).
27. Muzumdar, M. D., Tasic, B., Miyamichi, K., Li, L. & Luo, L. *Genesis* **45,** 593–605 (2007).
28. Wale, P. L. & Gardner, D. K. *Reprod. Biomed. Online* **21,** 402–410 (2010).
29. Sommer, C., Straehle, C., Kothe, U. & Hamprecht, F. A. in *Eighth IEEE International Symposium on Biomedical Imaging (ISBI)* **Proceedings,** 230–233 (2011).
30. Myronenko, A. & Song, X. *IEEE Trans. Pattern Anal. Mach. Intell.* **32,** 2262–2275 (2010).
31. Rossant, J. & Tam, P. P. L. *Dev. Cell* **7,** 155–164 (2004).
32. Rossant, J. & Tam, P. P. L. *Dev. Camb. Engl.* **136,** 701–713 (2009).
33. McDole, K., Xiong, Y., Iglesias, P. A. & Zheng, Y. *Dev. Biol.* **355,** 239–249 (2011).
34. Chen, B.-C. *et al. Science* **346,** 1257998 (2014).
35. Booth, M. J. *Light Sci. Appl.* **3,** e165 (2014).

Figure Legends

Figure 1 | Inverted light sheet microscope.

(**a**) Model of the microscope's sample mounting system: excitation light entry (Ex), sample positioning system (SP), illumination objective (IL), imaging objective (IM), flexible sealing ring (SR), immersion water reservoir (W), illumination and imaging objective mounting and positioning (ILP, IMP), emitted light exit (Em), mounting base plate (BP). (**b**) Model of the sample holder: transparent FEP membrane (M), embryo samples (S). (**c**) Model showing orientation of the objectives and the sample holder. Magnified view illustrates a drop of medium containing sample covered by mineral oil. Excitation light is shown in blue and emitted light in orange.

Figure 2 | Nuclei tracking from one cell stage to blastocyst.

(**a**) Live-cell time-lapse imaging of mouse pre-implantation embryos expressing H2B-mCherry (red) and mG (green, inset). Maximum intensity projections of selected frames along the z- (top) and the y-axis (bottom) are shown. Pronuclei (PN), metaphase (Met) and anaphase (Ana) are indicated by arrowheads. The cell surface marker (mG) was only imaged for the final division from 32 to ~64 cells. (**b**) 3D segmentation of embryo and nuclei surfaces at selected time-points. Polar body is shown in blue. (**c**) Nuclei segmentation and tracking pipeline. Individual 3D images from adjacent time-points are first segmented independently. The centers of segmented nuclei are then aligned with respect to each other and a tracking algorithm subsequently identifies the corresponding nuclei in both time-points and detects cell divisions. Polar body is marked by asterisk on the microscope images and is not shown in segmentation and tracking. (**d**) Tracking of nuclei from one cell stage to blastocyst. Maximum intensity projections of selected time-points are shown. Green spheres indicate the position of nuclei and their trajectories are shown in magenta. Note that a pair of pronuclei was tracked as one object. Scale bars apply to all images in a panel.

Figure 3 | Cell fate is biased towards ICM or TE lineage from 16-cell stage.

(**a**) Selected planes from the last time-point of nuclei tracking. The fluorescence signal of H2B-mCherry and mG was used to assign cells to TE or ICM lineage. (**b**) Live-cell time-lapse imaging of embryos expressing H2B-mCherry (white) and mG (not shown). Maximum intensity projections are shown. Relative contribution of each cell to the ICM (red) or TE (blue) lineage is shown by color coded spheres. (**c**) Lineage trees of mouse pre-implantation development from one cell stage to blastocyst. Percentage of ICM (red) or TE (blue) cells derived from each cell is displayed on the tree by color code. (**d**) Simplified representation of a lineage tree where cell fates at the bottom of the three are randomized. Color code represents how much a relative contribution of each branch to the ICM (red) or TE (blue) lineage deviates from the whole embryo average (white, visible at one cell stage). (**e**) Same lineage tree representation as in **c** but showing observed cell fates. (**f**) Probability that observed lineage segregation at 2-, 4-, 8-, 16- or 32-cell stage occurred by chance. Probability was estimated using a permutation test where observed tree was compared to 100,000 trees with randomized fates. (**g**) Distribution of probabilities described in panel **f** for all tracked embryos (n = 12) at 4-, 8-, 16- or 32-cell stages. Combined probability is shown inside the graph and was calculated by Fisher's combined probability test. Scale bars apply to all images in a panel. Polar body is marked by asterisk on all panels.

Online Methods

Optical Setup

Our inverted light sheet microscope (schematic shown in Supplementary Fig. 3) consists of the illumination arm (excitation laser beam shown in blue), imaging arm (emitted light shown in orange) and a sample mounting part with controlled atmosphere composition and temperature (dashed line). Laser beams from 488 nm (LuxX 488-60; Omicron-Laserage Laserprodukte) and 561 nm (Cobolt Jive, 50 mW; Cobolt) lasers are combined inside a laser combiner (LightHUB-6) and coupled into a single-mode optical fiber (kineFLEX; both Omicron-Laserage Laserprodukte). The intensity of the 488nm-laser diode is directly modulated (analog and digital input on the laser head) and the intensity of the 561 nm-laser is controlled by an acousto-optic modulator (Crystal Technologies, Inc. AOM Model 3080). A clean-up filter is placed in front of the 488 nm-laser to reduce the LED background. The laser beams are collimated at the exit of the optical fiber (0.7 mm beam diameter) and their intensity can be further attenuated by neutral density filters (NE10B, NE20B, NE30B, NE40B; Thorlabs) placed in a manual filter wheel (FW1A; Thorlabs). In order to adjust the light sheet thickness and length, the laser beam is split into two beams of roughly equal intensities using a polarizing beam splitter (PBS201; Thorlabs). While the diameter of one beam is doubled by a telescope (f = -50 mm, NT62-492-INK, f = 100 mm, NT47-641-INK; Edmund Optics), the diameter of the other beam remains unaffected. Both beams are aligned using kinematic mirrors (KM100-E02) and combined using polarizing beam splitter (PBS201; both Thorlabs). Switching between both beam diameters was performed by manually blocking one beam. The two beams resulted in a light sheet thickness (FWHM) of 3 µm and 1.5 µm for the thick and thin beam, respectively. The light sheet is created by scanning a focused laser beam (Nikon scan lens) with a galvanometric scanner (VM500+; General Scanning) in the imaging plane of an imaging pair consisting of a 10× 0.3 NA water immersion objective lens (CFI Plan Fluor 10XW) and a tube lens (f = 200 mm; both Nikon). The galvanometric scanner is mounted in a manual rotary support (G065088000; Qioptiq) allowing positioning of the light sheet into the focal plane of the imaging objective lens. The laser beam is directed to the back focal plane of the illumination objective by two mirrors (BB2-E02; Thorlabs) mounted in a custom designed aluminum objective holder block (Supplementary Fig. 1). Emitted fluorescence light is collected by a 100× 1.1 NA objective lens (CFI Plan 100XW; Nikon). The light is then directed by a mirror (BB2-E02; Thorlabs) mounted in a second custom designed objective holder block (Supplementary Fig. 1) to a motorized filter wheel (96A357; Ludl Electronic Products). An image is generated by a tube lens (f = 200 mm; Nikon) at an intermediate image plane where a circular aperture (FS) is placed to limit the field of view to 130 µm. The image is then demagnified four times using two relay lenses (f = 300 mm, 49-280-INK and f = 75mm, 47-639-INK; Edmund Optics) onto a sCMOS camera (Neo sCMOS; Andor). For some experiments an optional color splitter block consisting of two identical kinematic mirrors (POLARIS-K1 with BB1-E02; Thorlabs), two identical dichroic beam splitters (FF560-FDi01-25x36; Semrock) and two emission filters (BLP01-568R-25 and SEM-FF03-525/50-25; Semrock) was placed between the relay lenses to spectrally separate the image of EGFP and mCherry emission on the two sensor halves. In this configuration an empty filter position was selected on the motorized filter wheel. All components were mounted on an optical table using an optical rail system (Owis). Objective lenses are mounted in custom machined aluminum blocks on a linear translation stage (M-UMR5.16; Newport) with micrometric screws for precise alignment (Fig. 1A).

Sample mounting and positioning

Sample mounting in our inverted light sheet microscope is compatible with micro-drop culture commonly used to culture mouse embryos (see below). The sample holder (Fig. 1b) is made of medical grade plastic (PEEK; KTK). A 50 µm thin membrane (FEP; Katco; Fig. 1b) with a refractive index matching to the one of water is placed into a groove in the sample holder and sealed by a biocompatible silicone glue (Silpuran 4200; Wacker) applied to the bottom of the chamber at the interface between the chamber body and the membrane. The sample holder is placed inside the microscope into a three axis positioning system (Fig. 1a) made of custom aluminum adaptor blocks and three linear positioners (SLC-24; SmarAct). Because we used water dipping objectives a reservoir for immersion medium is filled with water so that both objectives and the bottom of the sample holder are below the water surface. To allow precise positioning of the objective lenses, flexible custom made polydimethylsiloxane (PDMS, SYLGARD 184; Dow Corning) rings were used as a seal between objective lenses and the water reservoir. The immersion medium reservoir together with positioners was partially sealed from surrounding atmosphere with a lid (not shown) to minimize water evaporation and a peristaltic pump was used to refill the water if needed while imaging was ongoing. The entire sample handling part of the microscope was enclosed in an environmentally controlled (37°C, 5% CO_2) incubator box (Supplementary Fig. 2, GP168 VII; EMBL electronic workshop).

Microscope control software

All microscope components were controlled by an in-house developed LabVIEW program (National Instruments). Precise timing of laser intensities, galvanometric scanner positions, and camera acquisition was ensured by a custom written program implemented in FPGA module (NI PCIe-7841R; National Instruments).

Mouse strains and embryo culture

Mouse embryos were collected from superovulated 8 to 12 weeks old female mice according to the guidelines of EMBL Laboratory Animal Resources and cultured in 10 - 20 µl drops of KSOM (KSOMaa Evolve; Zenith Biotech) covered by mineral oil (M8410; Sigma Aldrich). Embryos used for nuclei tracking were isolated from H2B-mCherry BL/6xC3H F1 females heterozygous for H2B-mCherry mated with mG BL/6xC3H F2 males heterozygous for mG transgene. The presence of both transgenes was evaluated at the end of time-lapse by looking for fluorescence signal from both transgenes. Embryos that did not develop to blastocyst stage, did not carry both transgenes or showed strong rotation during imaging were not tracked. Exclusion criteria were established before statistical analysis was conducted. All animals used in this study were form one group with the same genetic background and therefore no animal randomization or investigator blinding was applied.

Embryo imaging

All images were acquired with the above described in-house built inverted light sheet microscope. For nuclei tracking experiments 20 positions (1 embryo at each position) were imaged in parallel in seven independent imaging sessions. Stacks of 130 images with 1.040 µm between planes were acquired for the mCherry signal at each position at 5 min time intervals. The GFP signal was imaged approximately for the last 12 h of the time-lapse. For tracked embryos (n = 12) we have compared the division timing and number of total and ICM cells to values reported in the literature[12,28]. All values in this paragraph indicate mean ± standard deviation. The reported timing was recalculated with respect to 3-cell stage to be comparable with our data. In our dataset the timing for transition to 2-cell stage was 18 ± 1 h (19.6 h reported), to 4-cell stage 0.7 ± 0.4 h (0.8 h reported), to 8-cell stage 11.7 ± 1.5 h (12.8 h reported). The number of ICM cells and the total number of cells was reported at 30 h after compaction and in our study at the end of tracking which was 36 ± 3 h after transition to 8-cell stage. In our dataset the embryos contained 61 ± 4 total cells at this stage (60 ± 4 reported) and the number of ICM cells was 22 ± 4 (15 ± 5 reported). For confocal imaging (Zeiss LSM 780) embryos were imaged with the same temporal resolution (5 minutes) and z-stack settings (130 images with 1.040 µm between planes) and using the same laser wavelength (561 nm) as used for light sheet imaging. Control embryos were placed in an adjacent medium drop to the one with imaged embryos and handled identically. For maximum sensitivity a GaAsP detector was used and pinhole was opened to 2 airy units. Because embryos did not develop beyond 8 cell stage the GFP channel was not imaged and time-lapse was stopped. Out of 9 imaged embryos all were arrested around 8 cell stage. Out of 11 control embryos 10 developed to blastocyst stage.

Embryo transfer

20 embryos were imaged under conditions described above. Control embryos were cultured in an adjacent medium drop and treated identically. At the end of imaging 16 control as well as 16 imaged embryos at the blastocyst stage were transferred into day 2.5 pseudopregnant females (n = 2). Two round of embryo transfer were conducted. In the first round, 6 pups (2 males, 4 females) were born from the imaged embryos and 5 pups (2 males, 3 females) were born from the control embryos. No mice were born from control nor from imaged embryos in the second round of embryo transfer.

Image processing

Unless stated otherwise all image processing was done by custom written Python scripts that exclusively rely on functions from open-source Python libraries numpy, scipy, matplotlib, skimage and mahotas. EGFP and mCherry channels were first extracted from raw camera data containing signal for both channels on a single image (Supplementary Fig. 3). All images were then linearly scaled using a fixed minimum value and maximum value calculated in a way that a constant number of pixels is saturated on each time-point. Maximum intensity projections or images of a single plane are shown as indicated in figure legends. If indicated, image data were registered by applying a rigid body transformation that compensates for global drift or rotation of nuclei as well as additional transformation to rotate embryos in such a way that inner cell mass faces to the right. Nuclei coordinates and trajectories were rendered using PovRay 3.7 and overlaid on the maximum intensity projections.

Nuclei segmentation and tracking pipeline

In order to extract lineage tree information from the 4D light sheet datasets we developed an automatic segmentation and tracking pipeline (Fig. 2b). Individual 3D images from a time series were segmented using the machine learning software Ilastik (http://www.ilastik.org). The Ilastik classifier was trained by experts based on several representative 3D data sets across a single time series. This classifier was then applied to the entire time series of all 4D datasets. Where available, the second membrane channel was used to help separating densely packed nuclei at later stages of embryonic development. The prediction maps were converted to binary fore- and background images by applying automatically determined thresholds (using the Otsu method). The centroids of the 3D connected foreground regions were used as a proxy for nuclei positions at each time point (96% correct). Following segmentation, centroid datasets were aligned spatially by a coherent point drift method (https://sites.google.com/site/myronenko/research/cpd) to compensate for spatial drifts and rotations of the

embryo. These registered point sets were tracked using nearest neighbor association. Association failure indicated mitotic cell division. Mother-daughter assignment was done by searching for the pair of daughter centroids with minimal distance to the mother centroid (typically the center of the two daughter centroids coincided well with the position of the mother centroid). All nuclei positions and trajectories were validated manually. Reliable tracking (100% correct) was possible because throughout all datasets and time-points the mean spacing between nuclei centroids (52 μm) was much larger than the average distance nuclei movement between adjacent time-points (4 μm). During the manual validation all occurrences of cell death were annotated. Branches were then terminated in some embryos if individual blastomeres were lost due to cell death (Supplementary Fig. 5). This integrated segmentation and tracking pipeline enabled us to generate a fully verified lineage tree of the pre-implantation embryo within one day after image acquisition.

Cell lineage assignment

The last time-point of cell tracking was used to assign the ICM or TE fate to each cell. Nuclear and membrane signal was used to assign ICM fate to cells that had no contact to the embryo surface. Remaining cells were assigned to TE fate. This assignment was done by double blind fate scoring with > 97% agreement between the two experts. These fate assignments were then used for the lineage segregation analysis and both experts' results led to the same conclusions.

Statistical analysis of lineage segregation

To estimate a probability that the observed lineage segregation at a given time occurred by chance we have designed a permutation test which is described in details in Supplementary Note. Number of embryos used for the statistical analysis was fixed at the start of the experiment. No adjustment of sample size was applied.

Division angle estimation

The high spatio-temporal resolution of our inverted light sheet datasets facilitated a precise determination of the division axis orientation within the embryo for all division events across the entire embryo and observation time. The division angle (α in degrees) was calculated from the scalar product of the vector connecting the mother to the center of the embryo and the vector connecting the two daughter nuclei at the earliest time point the division could be detected. Due to symmetries the angle was restricted between 0° and 90° and calculated in such a way that cells dividing perpendicularly to embryo surface had division angle of 90° and cells dividing parallel to it 0°. A directional division angle was used where indicated. This angle is assigned to each daughter cell and it has a positive value of α degrees for daughter cells dividing towards the embryo center and negative value of $-\alpha$ degrees for daughter cells dividing towards the embryo surface. The embryo center was estimated as a center of mass of all nuclei coordinates in cases where the embryo had not started to cavitate. For embryos after cavitation onset, the center of mass of nuclei forming the convex hull was used. For divisions having random orientation, the division angle distribution is given by a cosine function. We performed Kolmogorov-Smirnov test to statistically evaluate deviation of our experimentally determined division angle distributions from the random case (stats.kstest method from Python scipy package was used).

Point spread function measurement

Fluorescent beads (100 nm TetraSpeck, T7279; Life Technologies) were immobilized in 1% agarose in water and imaged on our inverted light sheet microscope. The average image of 10 beads was calculated in ImageJ using 3D PSF estimator from the Mosaic package and is shown in Supplementary Fig. 4.

Code availability

All source code is available upon request.

Figure 1

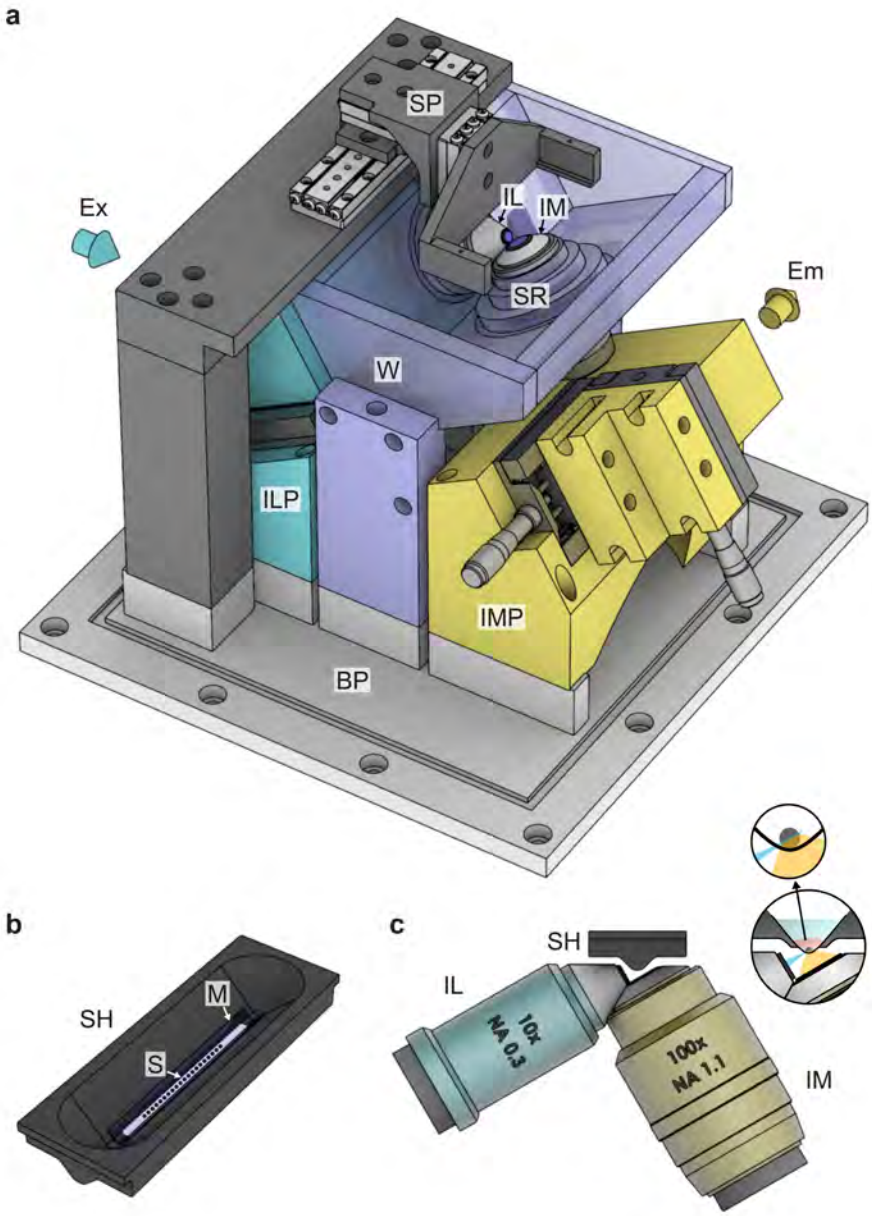

Figure 2

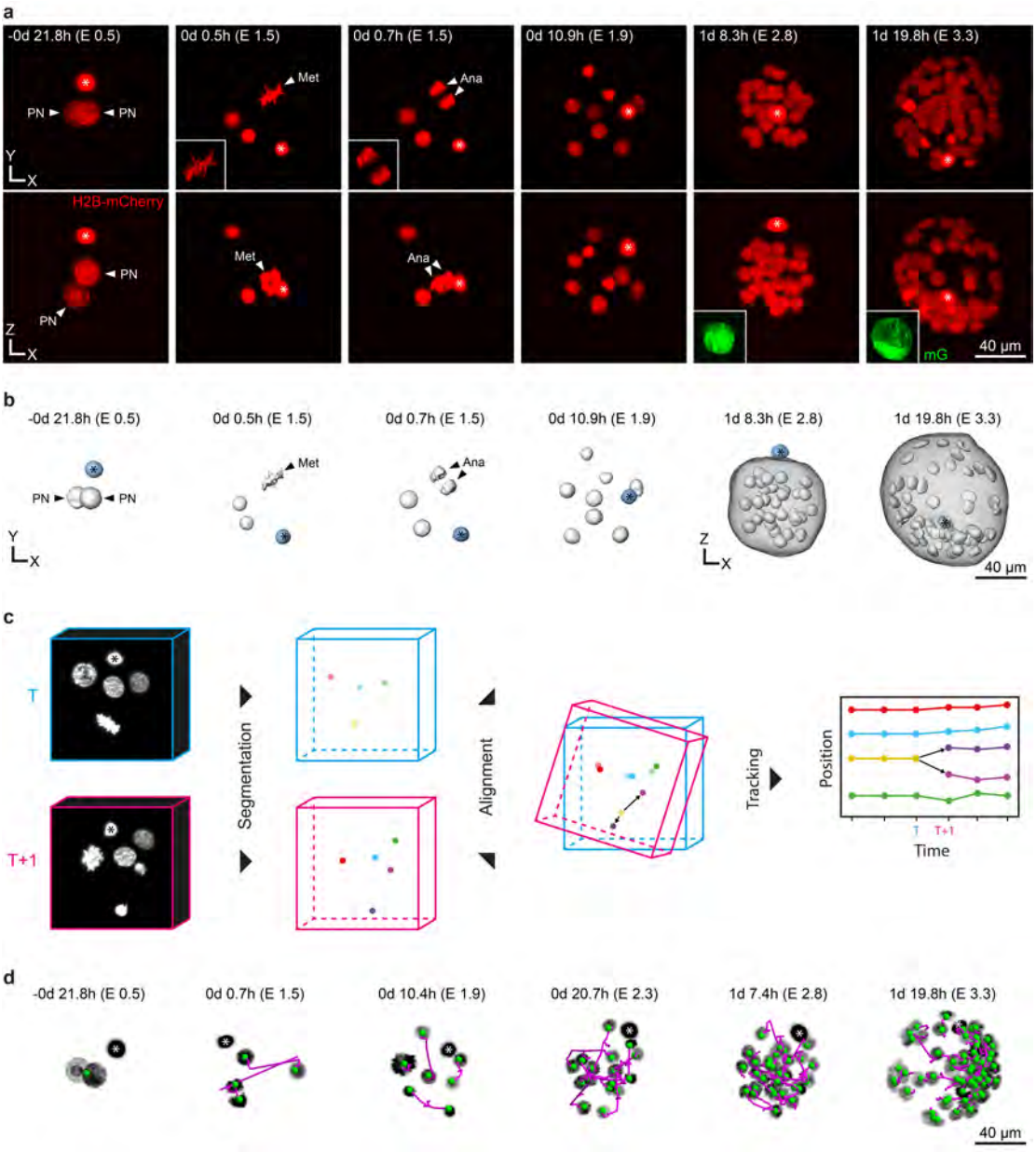
a
-0d 21.8h (E 0.5)
0d 0.5h (E 1.5)
0d 0.7h (E 1.5)
0d 10.9h (E 1.9)
1d 8.3h (E 2.8)
1d 19.8h (E 3.3)
PN
Met
Ana
H2B-mCherry
mG
40 μm
b
Segmentation
Alignment
Tracking
Position
Time
T
T+1
c
d
0d 10.4h (E 1.9)
0d 20.7h (E 2.3)
1d 7.4h (E 2.8)

Figure 3

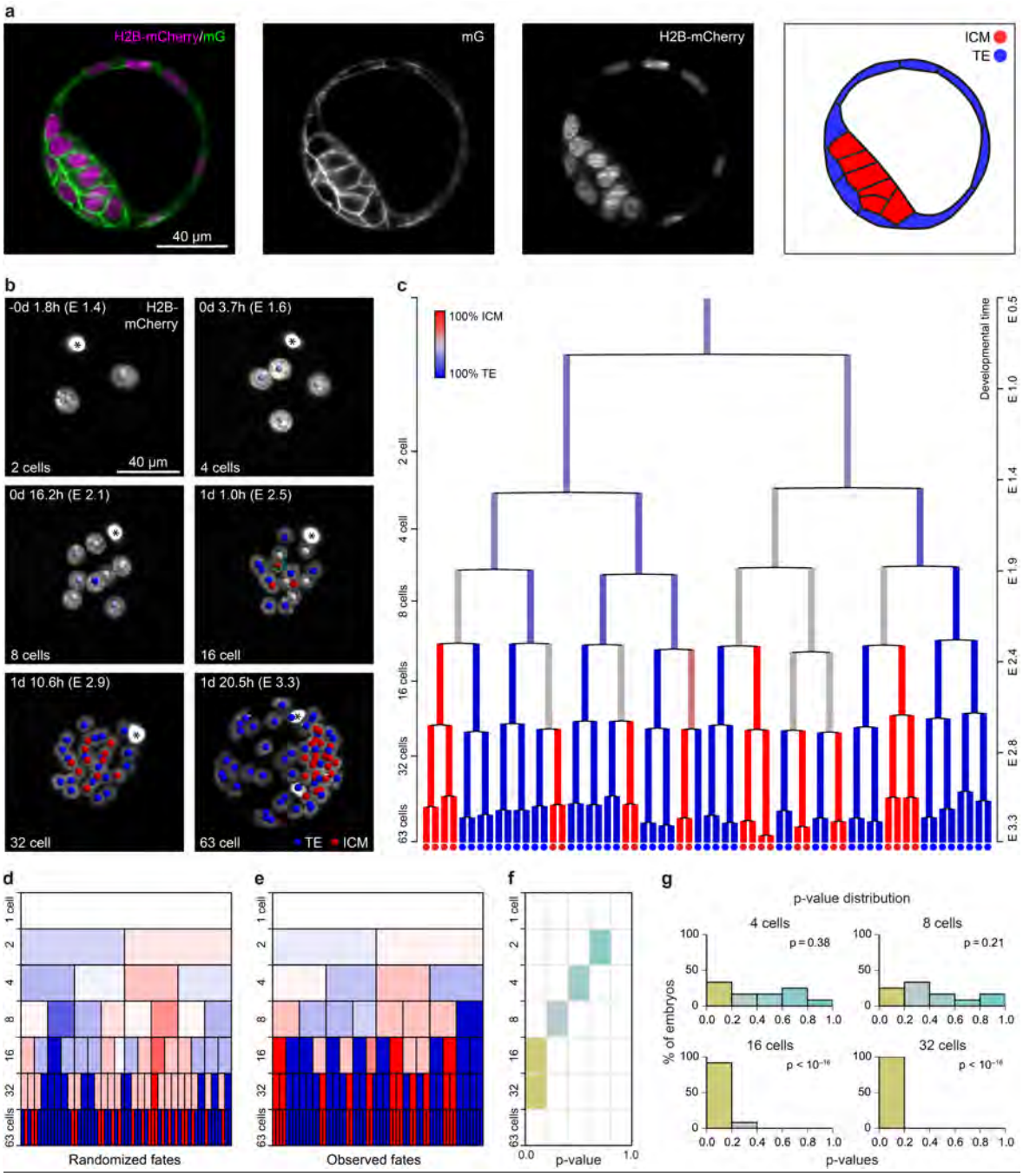
a
H2B-mCherry/mG
40 µm
mG
H2B-mCherry
ICM
TE
b
-0d 1.8h (E 1.4)
H2B-mCherry
2 cells
40 µm
0d 3.7h (E 1.6)
4 cells
0d 16.2h (E 2.1)
8 cells
1d 1.0h (E 2.5)
16 cell
1d 10.6h (E 2.9)
32 cell
1d 20.5h (E 3.3)
63 cell
TE
ICM
c
100% ICM
100% TE
2 cell
4 cell
8 cells
16 cells
32 cells
63 cells
Developmental time
E 0.5
E 1.0
E 1.4
E 1.9
E 2.4
E 2.8
E 3.3
d
1 cell
2
4
8
16
32
63 cells
Randomized fates
e
Observed fates
f
p-value
g
p-value distribution
4 cells
p = 0.38
8 cells
p = 0.21
16 cells
p < 10⁻¹⁶
32 cells
p < 10⁻¹⁶
% of embryos
p-values